Available online at www.sciencedirect.com
ScienceDirect
Journal of Molecular Catalysis A: Chemical 280 (2008) 52–60
JOURNAL OF MOLECULAR CATALYSIS A: CHEMICAL
www.elsevier.com/locate/molcata

Effects of support and metal loading on the characteristics of Co based catalysts for selective hydrogenation of citral

K. Kouachi [a,b], G. Lafaye [a,*], C. Especel [a], O. Cherifi [b], P. Marécot [a]

[a] Université de Poitiers, Laboratoire de Catalyse en Chimie Organique, UMR 6503, 86022 Poitiers, France
[b] Laboratoire de Chimie de Gaz Naturel, Faculté de Chimie, USTHB, BP 32, 16111 El Alia, Bab Ezzouar, Algeria

Received 20 August 2007; received in revised form 17 October 2007; accepted 17 October 2007
Available online 23 October 2007

Abstract

Silica-, alumina- and titania-supported Co catalysts with different metal loadings were tested for selective citral hydrogenation in liquid phase. Temperature programmed desorption of hydrogen (H_2-TPD) indicated that the catalysts with the highest unsaturated alcohols selectivities present particular H-Co species. Electron diffraction and XRD measurements revealed that these species would be linked to the presence of Co^0 hexagonal phase. According to the results obtained by TEM and cyclohexane dehydrogenation, these two properties would be present on large Co particles.

Keywords: Cobalt; Catalysts; Selective hydrogenation; Citral

1. Introduction

One important reaction in the production of fine chemicals is the selective hydrogenation of α,β-unsaturated aldehydes to unsaturated alcohols (UA). The selectivity to these alcohols is highly dependant on the nature of the metal used as a catalyst. Concerning the noble metals, Os, Ru and Ir generally exhibit high selectivity toward UA while Pt, Pd and Rh lead mostly to the formation of saturated aldehydes [1]. However, the addition of different modifiers (Sn, Ge, ...) on these latter monometallic systems [1–6] or the use of reducible supports allowed one to improve the selective hydrogenation of the C=O bond [7–17].

Among the non-noble metals, Co has been mainly used in catalysts with the presence of additives. For example, the combination of cobalt-boride [18] and cobalt-cerium [19] revealed high selectivity toward UA for citral and cinnamaldehyde hydrogenation, respectively. However, there are few reports about supported monometallic cobalt catalysts for the hydrogenation of α,β-unsaturated aldehydes. Singh and Vannice showed that Co/SiO_2 presents higher selectivity than the noble metals toward UA for citral hydrogenation [20]. Nitta et al. observed that the selectivity to UA increases with increasing the Co particle size of the catalyst for selective hydrogenation of cinnamaldehyde and crotonaldehyde [21,22]. Coq et al. have also demonstrated that Co has promising potential for acrolein hydrogenation [23]. Likewise, Ando et al. found high selectivity performance for Co/Al_2O_3 catalysts during selective hydrogenation of different unsaturated aldehydes [24]. Nevertheless, studies explaining the origin of the observed high selectivities are scarce. Bailie et al. [25], Rodrigues et al. [26,27] and Djerboua et al. [28] have shown that the superficial structure of Co supported on silica influences the hydrogenation of C=O bond to crotyl alcohol formation. There are very few reports on the hydrogenation of citral on supported cobalt systems [18,20]. This paper deals with the preparation of silica-, alumina- and titania-supported Co catalysts with different metal loadings. The catalysts were characterized using electron microscopy and diffraction, X-ray diffraction, temperature programmed desorption of H_2, and cyclohexane dehydrogenation. Their effectiveness for citral hydrogenation was examined, with the results suggesting several key attributes for achieving more optimal selectivity towards unsaturated alcohols.

2. Experimental

2.1. Catalyst preparation

Four different supports were used: SiO_2 with a low-surface-area (Aldrich, $4\,m^2\,g^{-1}$, denoted LS), SiO_2 with a

* Corresponding author.
E-mail address: gwendoline.lafaye@univ-poitiers.fr (G. Lafaye).

1381-1169/$ – see front matter © 2007 Elsevier B.V. All rights reserved.
doi:10.1016/j.molcata.2007.10.018

high-surface-area (Degussa, 200 $m^2\,g^{-1}$, denoted HS), γ-Al_2O_3 (Axens, 210 $m^2\,g^{-1}$) and TiO_2 (Degussa, 50 $m^2\,g^{-1}$). Prior to their use, they were ground and then sieved to retain particles with sizes between 0.04 and 0.10 mm. The supports were calcined in flowing air for 4 h at 500 °C.

Co catalysts with different metal loadings were prepared by wet impregnation of the supports at room temperature using an aqueous solution of $Co(NO_3)_2{\cdot}6H_2O$ (Merck). The water was slowly eliminated by evaporation in a rotary evaporator for 10 h. After impregnation, the catalysts were dried at 120 °C for 48 h and then reduced at 450 °C (heating rate = 2 °C min^{-1}) in flowing pure hydrogen for 12 h.

2.2. Transmission electron microscopy (TEM) and electron diffraction

The morphology of the catalysts was studied by transmission electron microscopy and by electron diffraction to determine the Co particle size and the phase composition over the different supports, respectively.

Transmission electron microscopy (TEM) studies were performed on a Philips CM 120 instrument operating at 120 kV. All the samples were embedded in a polymeric resin (spurr) and cut into a section as small as 40 nm with an ultramicrotome equipped with a diamond knife. Cuts were then deposited on an Al grid previously covered with a thin layer of carbon.

Electron diffraction patterns were obtained in the same electron microscope. Interreticular distances d_{hkl} as well as lattice parameters were calculated from the distances between the spots and the angles formed by the lines passing through these spots. A program [29] allows one to check the calculated values by drawing the theoretical pattern along the same zone axis and by comparing it to the experimental pattern.

2.3. Gas phase reaction

Cyclohexane dehydrogenation was carried out under atmospheric pressure in a continuous flow reactor at 300 °C. Injection of cyclohexane was made using a calibrated motor-driven syringe. The partial pressures were 97 and 3 kPa for hydrogen and cyclohexane, respectively. All measurements were performed with a total flow rate of 100 $cm^3\,min^{-1}$. Analysis of the reaction products was performed by gas chromatography with a flame ionization detector (Varian 3400X) on a HP-PLOT Al_2O_3 "KCl" column.

2.4. XRD measurements

Powder X-ray diffraction (XRD) patterns of various samples were recorded on a Siemens D-500 diffractometer. The diffractograms were performed with Cu Kα radiation (λ = 1.5404 Å) over a range of 2θ from 20° to 80° with a 0.04° step size. Crystalline phases were identified by comparison with the reference data from International Center for Diffraction Data (ICDD) files.

2.5. Temperature-programmed desorption of hydrogen (TPD-H_2) experiments

The temperature-programmed desorption of hydrogen (TPD-H_2) experiments were carried out using an U-shaped quartz reactor connected to a thermal conductivity detector. First, the samples were reduced in a 1.0 vol.% H_2/Ar gas mixture at 450 °C (heating rate = 5 °C min^{-1}) for 1 h. Once the catalysts were cooled down to room temperature, the surface was purged by flowing Ar for 1 h. Subsequently, temperature was linearly increased from room temperature to 350 °C at 5 °C min^{-1}, following the hydrogen desorption with the thermal conductivity detector. The amount of H-Co species was calculated from desorption peaks area obtained by Gaussian deconvolution of TPD-H_2 spectra.

2.6. Citral hydrogenation

The liquid phase hydrogenation of citral was carried out in a 300 mL stirred autoclave (Autoclave Engineers, fitted with a system for liquid sampling) at 90 °C and at constant pressure of 7 MPa. Before each catalytic experiment, the catalyst (400 mg) was reduced at the desired temperature for 1 h, then immersed into 90 mL of solvent (isopropanol 99%) without exposure to air before the transfer towards the autoclave. After a first flush with nitrogen and a second with hydrogen, the temperature was raised to 90 °C under 3 MPa of hydrogen. Then a mixture of substrate (3 mL of citral) and isopropanol (10 mL) was loaded into the autoclave through a cylinder under 7 MPa hydrogen pressure. Zero time was taken at this moment and stirring was switched on.

Liquid samples were analysed by gas chromatography on a Thermofinnigan chromatograph provided with a FID detector and a capillary column DB-WAX (J&W, 30 m, 0.53 mm i.d.) using nitrogen as carrier gas.

3. Results and discussion

3.1. Evaluation of the Co particle size

Selected supported-Co catalysts on the different oxides were characterized by TEM after reduction at 450 °C. Concerning the silica supports, Fig. 1a–d shows characteristic TEM images obtained for Co/SiO_2 LS and Co/SiO_2 HS catalysts, respectively. In both cases, these analyses reveal that the cobalt particles do not distribute homogeneously. The Co/SiO_2 LS catalysts (Fig. 1a and b) present large Co particles with a size in the range of 10–150 nm at low Co loading and from 10 up to 200 nm above 15 wt% Co. The Co/SiO_2 HS catalysts show quite different morphology, with the Co particles appearing in the shape of bi-dimensional aggregates on the support (Fig. 1c and d). The size and the number of the aggregates increase as the cobalt loading of the catalyst increases. Thus, at low loading (<10 wt% Co) the spherical aggregates measure from 10 to 100 nm and above 10 wt% Co, the aggregates are ≥200 nm. Riva et al. have observed the same phenomena on Co supported over amorphous Kieselgel 60 (Merck) sil-

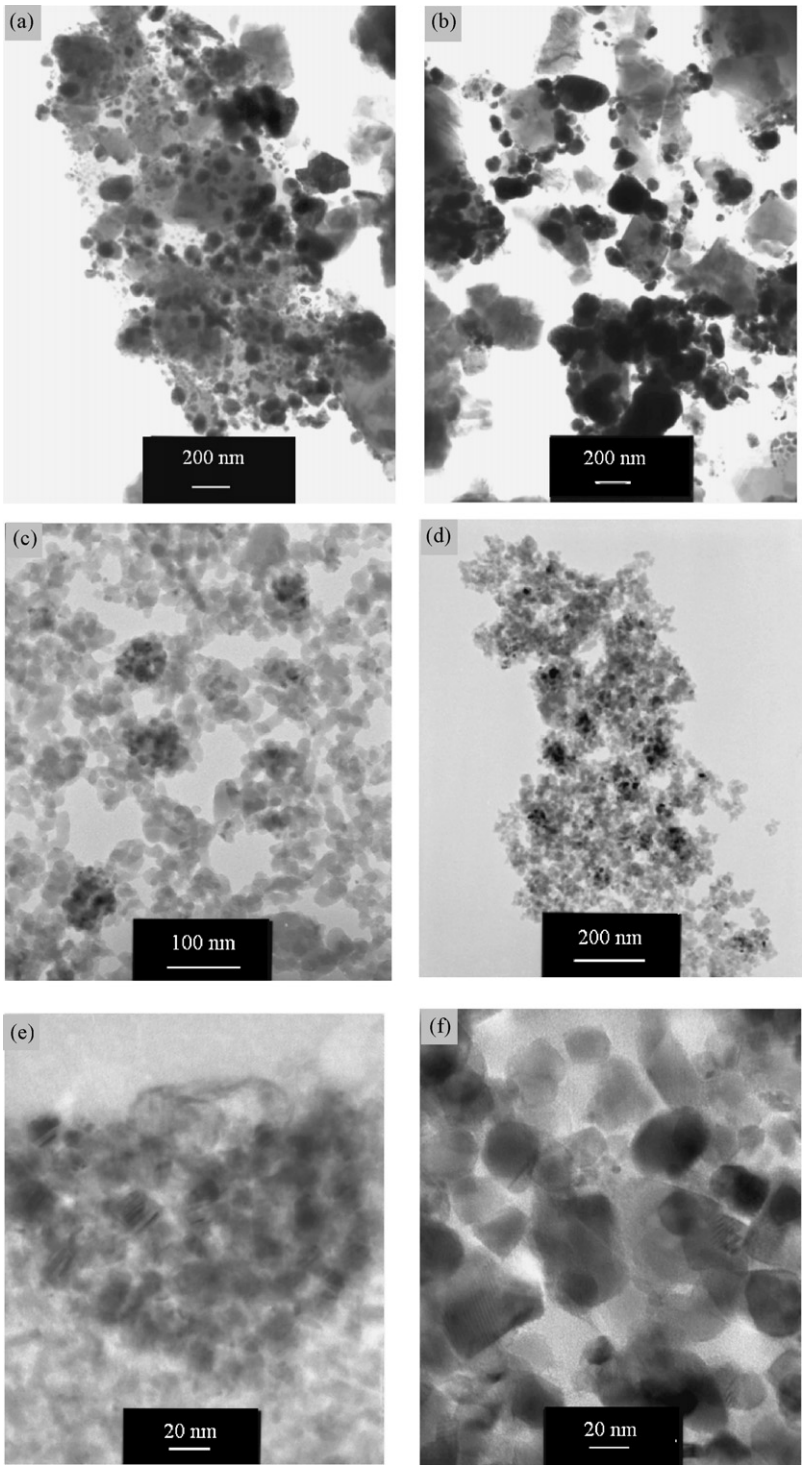

Fig. 1. TEM images of (a) 5 wt% Co/SiO_2 LS, (b) 15 wt% Co/SiO_2 LS, (c) 5 wt% Co/SiO_2 HS, (d) 10 wt% Co/SiO_2 HS, (e) 3.5 wt% Co/Al_2O_3 and (f) 3.5 wt% Co/TiO_2.

ica with a specific surface area of 430 $m^2\,g^{-1}$ [30]. At low loading (from 2 to 10 wt% Co), small (50–80 nm) spherical aggregates of cobalt phase were observed. Increasing the cobalt loading, the aggregates become larger (0.3–0.5 μ) and above 17–18 wt% Co, the aggregates reach micrometer dimensions [30]. Jabloński et al. have also observed these grape-like structures for Co/SiO_2 catalysts with high surface area silica (390 $m^2\,g^{-1}$), while the Co particles were rather uniformly distributed all over the support when using a low-surface-area silica (35 $m^2\,g^{-1}$) [31]. On the other hand, it appears in this work that for the same Co loading the particles are smaller on SiO_2 HS than on SiO_2 LS. This is reasonable since the SiO_2 HS presents a much higher surface area (200 $m^2\,g^{-1}$) than the SiO_2 LS (4 $m^2\,g^{-1}$).

It should be pointed out that it is well-known in the literature that most of the supported Co catalysts prepared by the impregnation method, involving either cobalt nitrates [32–40], or other salts such as chlorides [32,33,41,42] and acetates [32,33], exhibit low dispersion after reduction treatment. Usually, the average diameter of Co particles is in excess of 10 nm and the distribution width is generally large.

In the case of Co/Al_2O_3 (Fig. 1e) and Co/TiO_2 (Fig. 1f) catalysts, it was not possible to clearly distinguish Co particles. This problem has already been reported in the literature and explained by the fact that both the cobalt phases and the support materials reveal a crystalline structure [43]. Moreover, the atomic masses of Co and Ti do not differ considerably from one another, which explains the low contrast between the metal particles and the support for Co/TiO_2 samples [43].

The different catalysts were tested for cyclohexane dehydrogenation at 300 °C and atmospheric pressure. This structure insensitive reaction [44–46] was chosen in order to explore the evolution of the Co particle size with metal loading. This was particularly necessary for the Al_2O_3 and TiO_2 materials for which TEM was not effective. The cobalt particle size could not be determined by H_2 chemisorption because the amount of hydrogen adsorbed was too low for a reliable measurement to be made.

The evolution of the catalytic properties of all the Co based catalysts is shown in Fig. 2 as a function of the cobalt loading. From this figure it can be seen that whatever the nature of the support, the specific activity decreases as the Co content increases. This result indicates that the dispersion decreases as the Co content increases, consistent with formation of large Co particles. Moreover, the large difference of the specific activity observed at low and high Co contents for both silica series confirms that the mean particle size varies in a large range on these catalysts.

On the other hand, the comparison of the specific activities shows that, for a same Co content, the SiO_2 LS series is less active than the SiO_2 HS series. This difference supports the TEM results that the metal particles are larger on Co/SiO_2 LS than on Co/SiO_2 HS. As for alumina-supported samples, they are far less active than the SiO_2 HS ones despite the similar surface area of the supports (210 $m^2\ g^{-1}$ versus 200 $m^2\ g^{-1}$ for Al_2O_3 and SiO_2

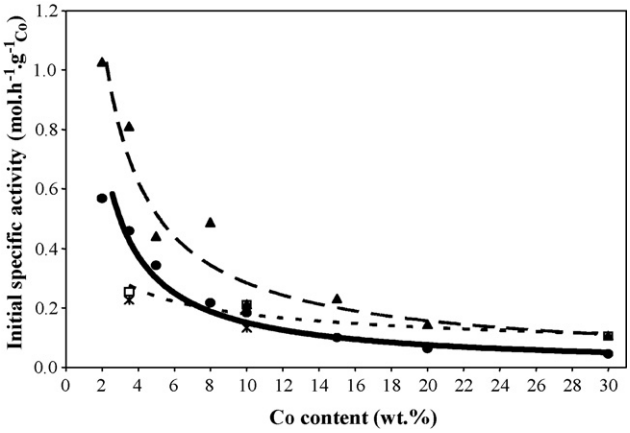

Fig. 2. Initial specific activity of cobalt supported catalysts for cyclohexane dehydrogenation at 300 °C as a function of Co content: (▲) Co/SiO_2 HS; (●) Co/SiO_2 LS; (□) Co/Al_2O_3; (×) Co/TiO_2.

HS, respectively). It has been reported in the literature that the cobalt interacts strongly with the alumina support. The reducibility of the cobalt is thus hindered by metal–support interaction, resulting in inferior catalytic properties [47,48]. Therefore, it is reasonable to assign the low activity of our Co/Al_2O_3 catalysts to the strong interaction between Co and Al_2O_3.

Likewise, the low specific activities observed for the titania-supported catalysts may result from the titania support that is partially reduced during the catalyst reduction step at high temperature (450 °C). This might then hinder one part of the active Co surface [30,49].

3.2. Determination of the Co phase composition

Electron diffraction analysis was performed during the TEM measurements on the SiO_2 supported catalysts. Fig. 3 gives examples of electron diffraction patterns for 10 wt% Co/SiO_2 HS. They consist of rings with superimposed diffraction spots. Table 1 summarizes the Co phase composition of the samples. It appears that both Co/SiO_2 LS and Co/SiO_2 HS catalysts present cubic (Fig. 3a) and hexagonal (Fig. 3b) metallic cobalt phases. The exception is Co/SiO_2 LS at a Co content ≤5 wt%, which

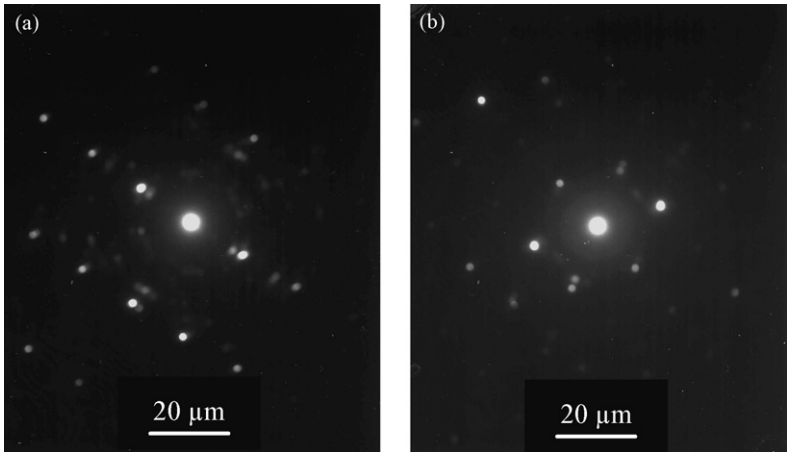

Fig. 3. Electron diffraction patterns for 10 wt% Co/SiO_2 HS catalysts: (a) Co^0 cubic phase and (b) Co^0 hexagonal phase.

Table 1
Co phase composition as a function of Co content

Support	Wt% Co	Co phase composition	
		Electron diffraction	XRD
SiO_2 LS	2.0	Co cubic	Co cubic
S = 4 $m^2.g^{-1}$	5.0		
	10	Co cubic + Co hexagonal	Co cubic + Co hexagonal
	↓ 30		
SiO_2 HS	3.5	Co cubic + Co hexagonal + CoO cubic	Co cubic + Co hexagonal + CoO cubic
S = 200 $m^2.g^{-1}$	↓ 30		
Al_2O_3	3.5		Co cubic + Co_3O_4
S = 210 $m^2.g^{-1}$	↓ 30		
TiO_2	3.5		Co cubic
S = 50 $m^2.g^{-1}$	10		Co cubic + Co hexagonal

does not present the Co hexagonal phase. On the other hand, the high-surface-area samples also reveal the presence of CoO crystallites.

X-ray powder diffractograms were performed on all the samples after reduction at 450 °C. The results are summarized in Table 1. Concerning the catalysts supported on silica, the diffraction patterns reveal quartz SiO_2 for LS and amorphous SiO_2 for HS, as expected. The XRD analysis confirms the results of the electron diffraction investigations, i.e.: (i) Co/SiO_2 LS with Co content >5 wt% and Co/SiO_2 HS catalysts consist of cubic and hexagonal metallic cobalt phases, (ii) Co/SiO_2 HS samples present also CoO crystallites. Riva et al. mentioned that for Co/SiO_2 containing from 2 to 27 wt% metal loading at high temperature (900 °C), the cobalt crystallizes as cubic metal. In contrast, at lower temperature (400 °C) a fraction of Co also crystallizes in the hexagonal form and some residual CoO is present, probably due to the passivation process [30].

Likewise, the signals obtained for the Co/TiO_2 series are assigned to cubic and hexagonal metallic cobalt phases for the highest Co loading (10 wt% Co) whereas only Co^0 cubic crystalline phase is present for the lower loading (3.5 wt% Co). In addition, a slight phase transfer of TiO_2 from anatase to rutile was observed in accordance with previous results [50,51].

In contrast with Co/SiO_2 LS and HS and Co/TiO_2, evaluation of the Co/Al_2O_3 diffraction results reveals that the samples consist only of Co^0 cubic and Co_3O_4 phases, regardless of Co content. No signal originating from Co hexagonal metallic phase was detected.

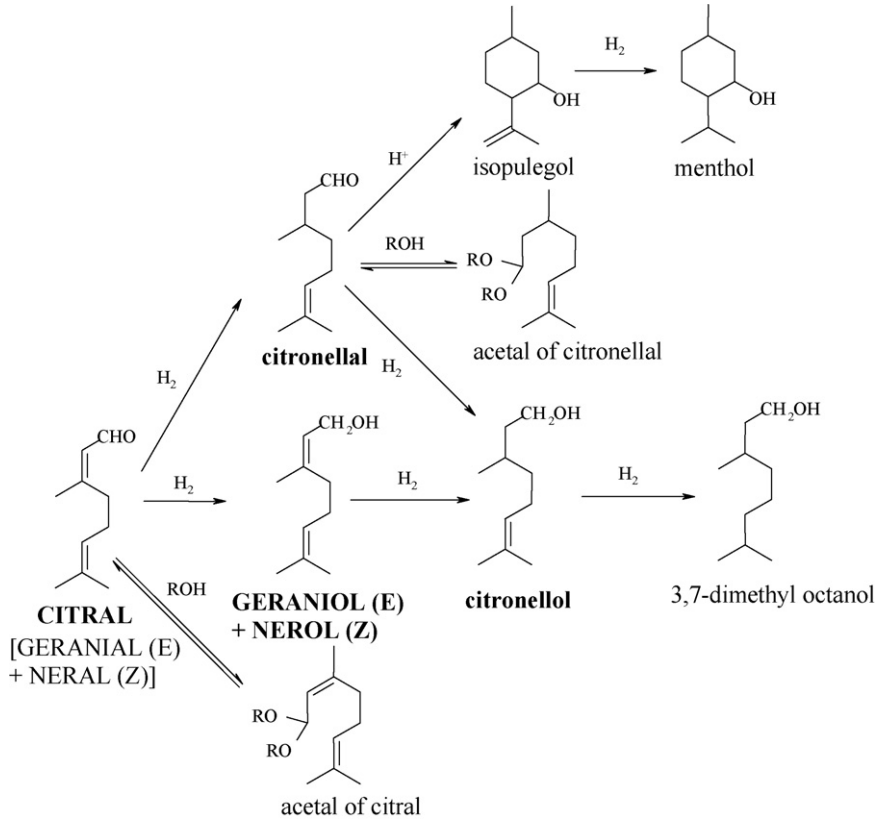

Fig. 4. Reaction scheme for citral hydrogenation.

3.3. Citral hydrogenation

The catalytic behavior of the samples in the liquid-phase hydrogenation of citral was evaluated after reducing in situ the catalysts at 450 °C. The hydrogenation of citral occurs through a reaction pathway which is summarized in Fig. 4. Regardless of the nature of the support or the metal loading, the reaction products were found to be: geraniol and nerol (unsaturated alcohols, UA), citronellal and citronellol. The side reactions, like acetalization or cyclization, were not observed. This result is explained by the fact that a chloride-free Co precursor was used for the preparation of the catalysts. It has been reported in the literature that the presence of chlorine in the course of citral hydrogenation often leads to by-products (e.g., isopulegols) [52].

Fig. 5 presents the citral conversion as a function of time during hydrogenation on the Co/SiO_2 HS series. As expected, the citral conversion increases with the cobalt content. The same result is obtained whatever the support, i.e. SiO_2 LS, Al_2O_3 and TiO_2. Moreover, whatever the support and the Co loading, significant catalyst deactivation was not observed, in contrast with previous results reported in the literature [20,53–58]. Generally, for the supported Group VIII metals, a rapid hydrogenation of citral occurs during the first few minutes, then the catalyst activity decreases after this earlier period. The explanation generally proposed, based on several kinetic and spectroscopic studies, is a decomposition of the citral or unsaturated alcohols yielding chemisorbed CO and carbonaceous species that accumulate on the catalyst surface and block a portion of the active sites [20,53,54]. The same phenomenon has been reported by Rodrigues and Bueno concerning crotonaldehyde hydrogenation in gas phase over Co/SiO_2 catalysts [55].

The initial specific activities of all the Co based catalysts are shown in Fig. 6 as a function of the cobalt loading. Concerning the silica and titania series, the decrease of the specific activity as the Co content increases is explained by the loss of dispersion. A different trend is observed for the Co/Al_2O_3 series since a significant gain in specific activity was obtained with the highest Co loading. This behavior can be attributed to a change in the degree of interaction of the cobalt species with the alumina. The increase in the average cluster size leads to a loss in interaction with the support, which induces an increase of the number of active sites. This result is in agreement with the work of Jacobs et al. [48]. They have demonstrated by TPR and H_2 chemisorption that increasing the average cluster size by increasing Co loading in Co/Al_2O_3 leads to a loss in interaction and then to improvements in the percentage reduction. This results in an increase of the availability of active surface Co atoms. On the other hand, the comparison of the specific activities displayed in Fig. 6 indicates that, for a same Co content, the Co/SiO_2 HS and Co/TiO_2 series exhibit a similar catalytic activity and are more active than the Co/SiO_2 LS and Co/Al_2O_3 series.

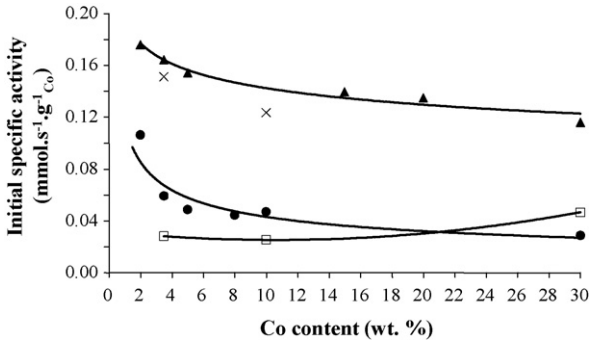

Fig. 6. Initial specific activity of cobalt supported catalysts for citral hydrogenation as a function of Co content: (▲) Co/SiO_2 HS; (●) Co/SiO_2 LS; (□) Co/Al_2O_3; (×) Co/TiO_2.

Fig. 7 presents a typical temporal concentration profile of the reactant and the main products during citral hydrogenation on the Co/SiO_2 HS. The reaction proceeds through two parallel routes leading to citronellal and the unsaturated alcohols. However, in the course of this C=C/C=O adsorption competition, Co tends to favor the C=O hydrogenation. Once the citral conversion reaches 100%, the UA continue to be hydrogenated into citronellol. It should be pointed out that the addition of H_2 to the isolated C=C does not occur under our experimental conditions. Therefore, the addition of hydrogen to citral takes place exclusively on the carbonyl group and on the conjugated C=C double bond. This result suggests that the citral molecules are adsorbed on the Co surface through the carbonyl or the conjugated C=C group, which adsorb preferentially to the isolated C=C. Chen et al. have also reported that citronellol was not further reduced to form the completely saturated product 3,7-dimethyloctanol in the course

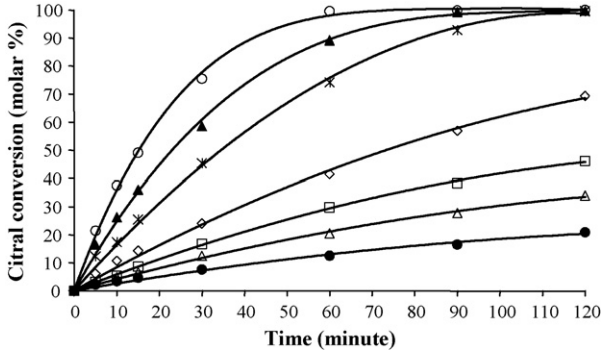

Fig. 5. Citral conversion as a function of time for the Co/SiO_2 HS series: (●) 2 wt% Co; (△) 3.5 wt% Co; (□) 5 wt% Co; (◊) 10 wt% Co; (×) 15 wt% Co; (▲) 20 wt% Co; (◯) 30 wt% Co.

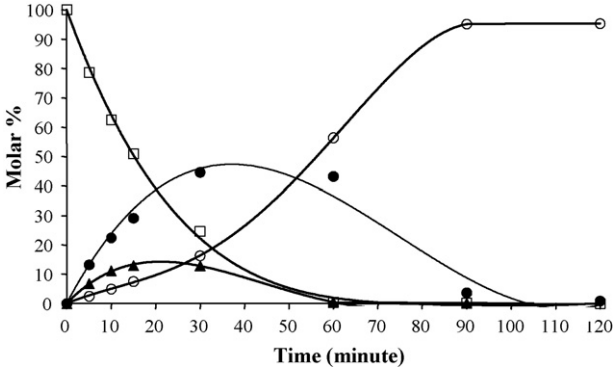

Fig. 7. Hydrogenation of citral on 30 wt% Co/SiO_2 HS catalysts: (□) citral; (▲) citronellal; (◯) citronellol; (●) unsaturated alcohols.

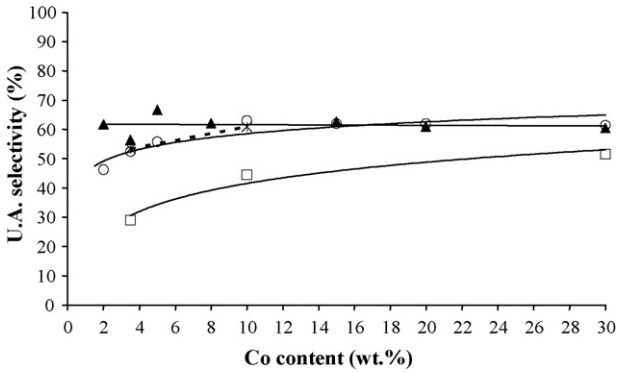

Fig. 8. Unsaturated alcohols selectivity at 30% citral conversion as a function of Co content: (▲) Co/SiO_2 HS; (◯) Co/SiO_2 LS; (□) Co/Al_2O_3; (×) Co/TiO_2.

of citral hydrogenation over Raney cobalt and CoB catalysts [18].

Fig. 8 displays the UA selectivity as a function of the cobalt content for the silica, alumina and titania series. The selectivity values are given at 30% citral conversion, although the same results are found over a large range of conversions. Concerning the SiO_2 LS, Al_2O_3 and TiO_2 supported catalysts, the UA selectivity increases with the cobalt content, with the SiO_2 LS series reaching a plateau at a Co content of 10 wt%. The increase of UA selectivity with the Co content of the samples could be related to the formation of large Co particles. Indeed, it has been shown that the selectivity to UA increases with increasing the metallic particle size of the catalyst for selective hydrogenation of different unsaturated aldehydes. For example, this effect was observed for Pt on various supports [56,57,11] and for Co/SiO_2 [21,22]. However, for the SiO_2 HS series the selectivity to UA remains almost constant regardless of the Co loading, i.e. regardless of the size of the Co crystallites. The increase of the Co particle size is thus not sufficient to explain the overall behavior of our systems.

From the XRD results summarized in Table 1, another hypothesis can be drawn. It appears that the Co^0 hexagonal phase can be detected at all Co loadings for SiO_2 HS, but only at or above 10 wt% Co for SiO_2 LS and TiO_2. Comparison of the Co samples shows that from 10 wt% Co content the catalysts have similar UA selectivity, with the exception of the Co/Al_2O_3 series whose UA selectivities are lower. Thus, the UA selectivity seems to be influenced by the presence of the Co^0 hexagonal phase and its relative proportion. Nevertheless, in the X-ray diffraction patterns of Co/Al_2O_3 it was not possible to detect signals originating from Co^0 hexagonal. A possible explanation of this observation would be that the Co^0 signals would be hidden behind the alumina signals of strong intensity.

Rodriguez et al. have drawn a correlation between the surface structure of Co/SiO_2 [26,55] and $ZnO–Co/SiO_2$ [27] catalysts (via TPD of hydrogen) and the hydrogenation product selectivity for crotonaldehyde hydrogenation in gas phase. Following these lines, the present Co supported catalysts were characterized by TPD of hydrogen (TPD-H_2) to determine if the same kind of correlation could be drawn with citral hydrogenation in liquid phase.

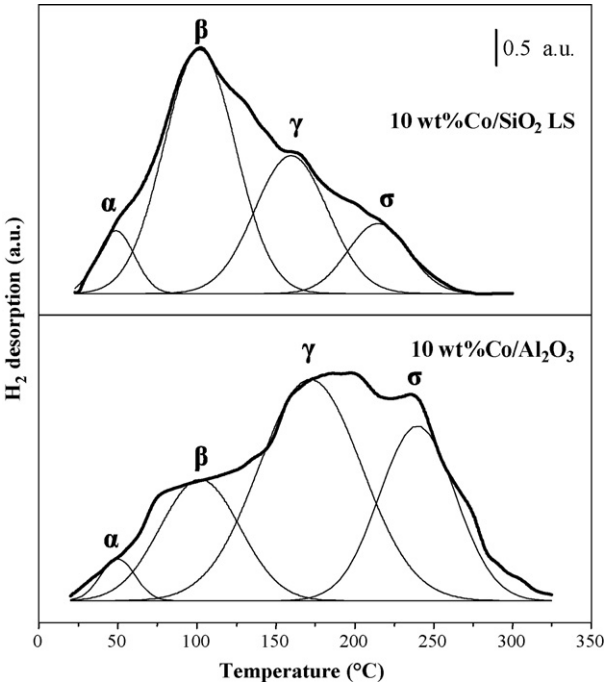

Fig. 9. H_2-TPD profiles of 10 wt% Co supported catalysts.

Two examples of TPD-H_2 profiles (10 wt% Co/SiO_2 LS and 10 wt% Co/Al_2O_3) are depicted in Fig. 9. In the case of Co/TiO_2 catalysts, the reducibility of the support prevents a determination of the Co surface by means of hydrogen desorption. The TPD-H_2 profiles of Co supported over silica and alumina present peaks located around 50, 100, 120–160 and 160–300 °C. Rodriguez et al. have demonstrated the presence of at least four different H-Co surface sites on silica, labelled α (peak at 50 °C), β (peak at 100 °C), γ (peak at 120–160 °C) and σ (peak at 160–300 °C) [26,27,55]. In agreement with this prior work, the same assignments are made for the present peaks on Co/silica. It also is reasonable to extend these assignments to alumina-supported Co catalysts since similar desorption peaks have been observed [58].

Table 2 summarizes the relative amounts of these various H-Co species, calculated by Gaussian deconvolution. It appears that the distribution of the different H-Co sites is strongly dependent on the nature of the support and on the Co loading of the catalysts. The best correlation between the selectivities to the different products (UA, citronellal and citronellol) and the

Table 2
Relative amounts of H-Co species in different Co-supported catalysts

Catalyst	Hydrogen species (%)			
	α	β	γ	σ
3.5 wt% Co/SiO_2 LS	60	28	12	0
10 wt% Co/SiO_2 LS	7	51	29	13
3.5 wt% Co/SiO_2 HS	10	45	26	19
10 wt% Co/SiO_2 HS	8	47	34	11
10 wt% Co/Al_2O_3	4	20	48	28
30 wt% Co/Al_2O_3	2	30	34	34

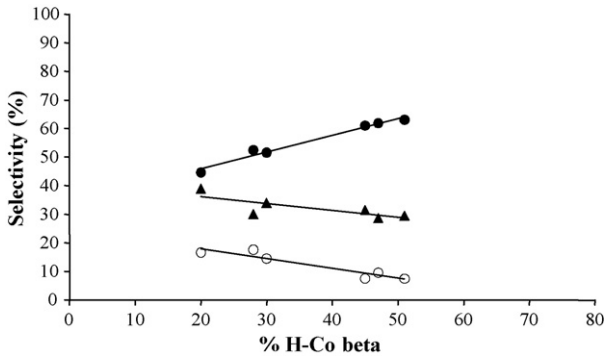

Fig. 10. Correlation between the selectivities and the percentage of the hydrogen species labelled β. Data obtained at 30% citral conversion, (●) unsaturated alcohols; (▲) citronellal; (◯) citronellol.

H-Co species present was obtained with the sites responsible for adsorption of hydrogen species labelled β. This correlation is given in Fig. 10. It indicates that the selectivity to UA, citronellal and citronellol are influenced by the percentage of these sites. The selectivity to UA increases with increasing percentage β with a corresponding decrease in the selectivity to citronellal and citronellol. Therefore, the β sites seem to be the key factor for C=O hydrogenation since they favor the C=O hydrogenation for crotonaldehyde hydrogenation in gas phase [27,55] as well as for citral hydrogenation in liquid phase.

4. Conclusion

Co catalysts with different metal loadings were prepared by wet impregnation of four different supports: SiO_2 with a low-surface-area, SiO_2 with a high-surface-area, γ-Al_2O_3 and TiO_2. All these systems were reduced at 450 °C and tested for the selective hydrogenation of citral. From the different characterization methods the following conclusions can be made:

- Temperature programmed desorption of hydrogen (H_2-TPD) revealed that the samples with the highest unsaturated alcohols selectivities present particular H-Co species, labelled β.
- Electron diffraction and XRD measurements indicated that the unsaturated alcohols selectivity seems to be influenced by the presence of the Co^0 hexagonal phase.
- TEM and cyclohexane dehydrogenation suggested that large Co particles favor the hydrogenation of the carbonyl group.

These three points would suggest a link between the presence of Co^0 hexagonal phase and the existence of β sites, and these two properties would be present on large Co particles. Thus, the next step of this work will be to develop a preparation method which allows one to obtain mainly Co^0 hexagonal phase across the support. The characterization of this material and its catalytic performances for the selective citral hydrogenation reaction will then provide further insight into this structure–selectivity relationship.

References

[1] P. Gallezot, D. Richard, Catal. Rev. 40 (1998) 81.
[2] B. Didillon, A. El Mansour, J.P. Candy, J.P. Bournonville, J.M. Basset, Stud. Surf. Sci. Catal. 59 (1991) 137.
[3] B. Didillon, J.P. Candy, F. Lepeltier, O.A. Feretti, J.M. Basset, Stud. Surf. Sci. Catal. 78 (1993) 147.
[4] G.F. Santori, M.L. Casella, G.J. Siri, H.R. Aduriz, O.A. Ferretti, Appl. Catal. A 197 (2000) 141.
[5] J.N. Coupe, E. Jordão, M.A. Fraga, M.J. Mendes, Appl. Catal. A 199 (2000) 45.
[6] G. Lafaye, C. Micheaud-Especel, C. Montassier, P. Marécot, Appl. Catal. A 230 (2002) 19.
[7] G. Lafaye, T. Ekou, C. Micheaud-Especel, C. Montassier, P. Marécot, Appl. Catal. A 257 (2004) 107.
[8] M.A. Vannice, B. Sen, J. Catal. 115 (1989) 65.
[9] M. Boutonnet Kizling, C. Bigey, R. Touroude, Appl. Catal. A 135 (1996) L13.
[10] D. Poondi, M.A. Vannice, J. Mol. Catal. A 124 (1997) 79.
[11] M. Englisch, A. Jentys, J.A. Lercher, J. Catal. 166 (1997) 25.
[12] M.A. Vannice, D. Poondi, J. Catal. 169 (1997) 166.
[13] P. Claus, S. Schimpf, R. Schödel, P. Kraak, W. Mörke, D. Hönicke, Appl. Catal. A 165 (1997) 429.
[14] U.K. Singh, M.A. Vannice, J. Mol. Catal. A 163 (2000) 233.
[15] R. Malathi, R.P. Viswanath, Appl. Catal. A 208 (2001) 323.
[16] P. Reyes, H. Rojas, J.L.G. Fierro, Appl. Catal. A 248 (2003) 59.
[17] T. Ekou, A. Vicente, G. Lafaye, C. Especel, P. Marécot, Appl. Catal. A 314 (2006) 73.
[18] Y.Z. Chen, B.J. Liaw, S.J. Chiang, Appl. Catal. A 284 (2005) 97.
[19] J. Barrault, A. Derouault, O. Martin, S. Pronier, C. R. Acad. Sci. Paris, Series IIC 2 (1999) 507.
[20] U.K. Singh, M.A. Vannice, J. Catal. 199 (2001) 73.
[21] Y. Nitta, K. Ueno, T. Imanaka, Appl. Catal. A 56 (1989) 9.
[22] Y. Nitta, Y. Hiramatsu, T. Imanaka, J. Catal. 126 (1990) 235.
[23] B. Coq, F. Figueras, P. Geneste, C. Moreau, P. Moreau, M. Warawdekar, J. Mol. Catal. A 78 (1993) 211.
[24] C. Ando, H. Kurokawa, H. Miura, Appl. Catal. A 185 (1999) L181.
[25] J.E. Bailie, G.J. Hutching, H.A. Abdullah, J.A. Anderson, C.H. Rochester, Phys. Chem. Chem. Phys. 2 (2000) 283.
[26] E.L. Rodrigues, A.J. Marchi, C.R. Apesteguia, J.M.C. Bueno, Stud. Surf. Sci. Catal. 130 (2000) 2087.
[27] E.L. Rodriguez, J.M.C. Bueno, Appl. Catal. A 257 (2004) 201.
[28] F. Djerboua, D. Benachour, R. Touroude, Appl. Catal. A 282 (2005) 123.
[29] C. Boudias, D. Monceau, Carine Crystallography Software, Version 3.1 (1989–1998).
[30] R. Riva, H. Miessner, R. Vitali, G. Del Piero, Appl. Catal. A 196 (2000) 111.
[31] J.M. Jabłoński, J. Okal, D. Potoczna-Petru, L. Krajczyk, J. Catal. 220 (2003) 146.
[32] T. Matsuzaki, K. Takeuchi, T.A. Hanoaka, H. Arakawa, Y. Sugi, Appl. Catal. A 105 (1993) 159.
[33] T. Matsuzaki, K. Takeuchi, T.A. Hanoaka, H. Arakawa, Y. Sugi, Catal. Today 28 (1996) 251.
[34] R.C. Reuel, C.H. Bartholomew, J. Catal. 85 (1984) 63.
[35] D.G. Gastner, P.R. Waston, I.Y. Chan, J. Phys. Chem. 94 (1990) 819.
[36] S. Halborsen, Stud. Surf. Sci. 61 (1991) 281.
[37] E. Iglesia, S.L. Soled, R.A. Fiato, J. Catal. 137 (1992) 212.
[38] E. Iglesia, S.L. Soled, R.A. Fiato, G.A. Via, J. Catal. 143 (1993) 345.
[39] G.J. Haddad, B. Chen, J.G. Goodwin, J. Catal. 160 (1996) 43.
[40] M.K. Niemelä, O.I. Krause, T. Vaara, J.J. Kiviacho, M.K.O. Rainikainen, Appl. Catal. A 147 (1996) 325.
[41] K. Takeuchi, T. Matsuzaki, T.A. Hanaoka, H. Arakaura, Y. Sugi, J. Mol. Catal. 55 (1989) 361.
[42] M.P. Rosynek, C.A. Polansky, Appl. Catal. 73 (1991) 97.

[43] M. Voß, D. Borgmann, G. Wedler, J. Catal. 212 (2002) 10.
[44] J.A. Cusumano, G.W. Dembinski, J.H. Sinfelt, J. Catal. 5 (1966) 471.
[45] D.W. Blakely, G.A. Somorjai, J. Catal. 42 (1976) 181.
[46] R. Ramos, A. Guerrero-Ruiz, J. Catal. 135 (1992) 458.
[47] S. Bessell, Appl. Catal. A 96 (1993) 253.
[48] G. Jacobs, T.K. Das, Y. Zhang, J. Li, G. Racoillet, B.H. Davis, Appl. Catal. A 233 (2002) 263.
[49] K. Suriye, P. Praserthdam, B. Jongsomjit, Catal. Commun. 8 (2007) 1772.
[50] K. Nagaoka, K. Takanabe, K. Aika, Appl. Catal. A 268 (2004) 151.
[51] K. Takanabe, K. Nagaoka, K. Nariai, K. Aika, J. Catal. 232 (2005) 268.
[52] P. Mäki-Arvela, L.P. Tiainen, A.K. Neyestanaki, R. Sjöholm, T.K. Rantakylä, E. Laine, T. Salmi, D.Y. Murzin, Appl. Catal. A 237 (2002) 181.
[53] S. Nishiyama, T. Hra, S. Tsuruya, M. Masai, J. Phys. Chem. 103 (1999) 4431.
[54] U.K. Singh, M.A. Vannice, J. Catal. 191 (2000) 165.
[55] E.L. Rodriguez, J.M.C. Bueno, Appl. Catal. A 232 (2002) 147.
[56] M.A. Vannice, Catal. Today 12 (1992) 255.
[57] M.A. Vannice, Top. Catal. 4 (1997) 241.
[58] L.B. Backman, A. Rautiainenb, M. Lindbladb, A.O.I. Krausea, Appl. Catal. A 191 (2000) 55.